

Characterizing the Vertical-to-Horizontal Ratio of Ground Motion at Soft-Sediment Sites

by Valerio Poggi, Benjamin Edwards, and Donat Fäh

Abstract A predictive equation to obtain the vertical-to-horizontal ratio (V/H) of ground motion for rock sites has been established in a previous article. The method was based on the comparison between V/H of Fourier and response spectra of earthquakes with the quarter-wavelength average velocity at discrete frequencies. We extend this approach to account for resonance phenomena at soft-sediment sites. In order to do so, a new parameter is defined and included in the comparison with the V/H spectra. The new parameter is directly derived from the quarter-wavelength velocity and represents the frequency-dependent seismic impedance contrast at the site. We show that extending the correlation in this three-dimensional space is beneficial to reconstruct V/H of the 5%-damped response spectra at soft-sediment sites ($V_{S30} < 800$ m/s) for which a shear-wave velocity profile is available. In this study we analyze 220 sites of the Japanese KiK-net strong-motion network. These sites were selected from the entire network through comparison of the fundamental frequencies estimated from the recordings and by indirect modeling methods. From the analysis, two types of predictive equations are then established, the first based on frequency-dependent and the second on frequency-independent correlations. These can subsequently be used to reconstruct the V/H spectrum at any site with a known shear-wave velocity profile. For both equations, uncertainties of the V/H models are provided, and a sensitivity study to magnitude–distance dependence is presented. Finally, we show an example of the application of the model at four selected soft-sediment sites of the Swiss Seismic Network.

Introduction

Despite recent evidence of its relevance in the action on particular structures such as highway bridges (e.g., [Kunnath *et al.*, 2008](#); [Gürlerce and Abrahamson, 2010](#)), the prediction of the vertical component of motion during an earthquake has so far mostly been estimated by indirect methods. In practice, direct modeling of the vertical design response spectra is generally possible using vertical ground-motion prediction equations ([Campbell, 1997](#)). However, in this case the earthquake disaggregation scenario might result in some inconsistencies with respect to the horizontal component prediction. To account for this problem, the suggested approach (e.g., [Gürlerce and Abrahamson, 2011](#)) consists of establishing a V/H conversion ratio for discrete spectral ordinates and for a set of source- and site-specific parameters, such as magnitude range, distance, and soil classification (e.g., [Bommer *et al.*, 2011](#)). In this way, only the horizontal conditional mean spectrum (CMS) ([Baker and Cornell, 2006](#)) has to be computed through a probabilistic approach. The vertical spectrum can be obtained subsequently through multiplication of the CMS with the V/H ratio, adjusting for the covariance of V/H and the horizontal spectral ordinates ([Gürlerce](#)

[and Abrahamson, 2011](#)). This approach presents a clear advantage in producing a homogeneous scenario for earthquake disaggregation for both the horizontal and the vertical design spectra.

In a recent study by [Edwards *et al.* \(2011\)](#), it was shown that the horizontal-to-vertical ratio of the ground motion for both Fourier and 5%-damped response spectra (in pseudo-spectral acceleration) can be directly linked to the local shear-wave velocity profile for sites with average velocity higher than about 800 m/s (rock sites). To link the velocity estimates with given spectral ordinates, the quarter-wavelength approach ([Joyner *et al.*, 1981](#); [Boore, 2003](#); [Poggi *et al.*, 2011](#)) was used to compute average velocities. The advantage of such a procedure is indeed the possibility of relating the depth over which the average velocity will be computed to a specific wavelength and—for a given velocity profile—to a specific frequency. The approach proposed by [Edwards *et al.* \(2011\)](#) was successful for those sites with rather high fundamental frequency f_0 , roughly above 10–15 Hz, characteristic of rock sites with a thin layer of weathered rock. While this generally limited their approach

from application to typical soft-sediment sites where most of the buildings are located, it may still play a role for sites of special structures such as dams, or for the cases of theoretical rock sites, often employed in probabilistic seismic hazard studies (e.g., Delavaud *et al.*, 2012). Below f_0 the contribution of body waves in the total wave-field composition is significant (Scherbaum *et al.*, 2003). Around and above f_0 , however, and particularly for those soft-sediment sites with a large contrast of velocity at depth, the influence of resonance phenomena and the generation of surface waves are important. This, therefore, will affect V/H ratios, which in this case depend not only on average velocity estimates from the profile but also on the impedance contrasts.

In this paper we present a method to estimate the V/H ground-motion ratio of soft-sediment sites, which is currently implemented in a national seismic hazard SSHAC Level 4 project in Switzerland. The proposed approach extends the previous methodology from Edwards *et al.* (2011) to also account for the amplification effects due to resonance phenomena as well as of increased presence of surface waves. To do so, a new parameter of the profile is introduced in the comparison with observed V/H ratios: the quarter-wavelength seismic impedance contrast, IC^{qw} , is based on the estimation of the contrast of seismic velocity that a wave of given frequency can resolve at the corresponding quarter-wavelength depth. Such a parameter has been introduced in the correlation with the observed V/H and quarter-wavelength velocity representation (V_S^{qw}) of the measured shear-wave velocity profiles. As a result of the correlation analysis, regression coefficients are then provided for a set of discrete frequencies in the range between 0.5 and 20 Hz.

With respect to previously proposed V/H models, the practical advantage of using such an approach is the possibility of obtaining a more accurate representation of the V/H function, which does not only depend on a single-site condition estimator (like the V_{S30} or a geotechnical class) as it is common in the engineering practice. It is important to notice that for a given V_{S30} , the influence of the soil resonance can be considerably different, according to the different soil properties at depth. This leads to a wide range of shapes of the V/H function for the same V_{S30} value. On the other side, the accuracy of the proposed procedure is at the expense of its implementation complexity. It is clear that the accuracy of the final result will mostly be driven by the reliability and extension of the available shear-wave velocity profile up to a sufficient depth, the retrieval of which is nowadays the major limitation in engineering site characterization studies. Nevertheless, the approach allows a more physically based estimation of the V/H ratio, given the best available information for the site of interest.

The presented method was calibrated and tested on a selection of sedimentary sites of the Japanese KiK-net seismic network. We show how the results of this analysis can be used in a general way to reconstruct the V/H function between 0.5 Hz and peak ground acceleration (PGA) of any sites with velocity profile of sufficient depth. We finally

study the magnitude–distance dependence of the V/H relation, based on residual analysis between computed and observed V/H ratios. The residual analysis also allows us to quantify uncertainties in terms of within- and between-event terms, which leads to estimates of single-site sigma (Atkinson, 2006). As an example of this application, the method has been applied to the site of permanent seismic station locations in Switzerland, for which measured velocity profiles and V/H ratios are available.

The Quarter-Wavelength Seismic Impedance Contrast

Using the quarter-wavelength average velocity (Joyner *et al.*, 1981) alone is not sufficient to characterize the variability of the V/H ground-motion ratio at soft-sediment sites. Spectral amplification, induced by vertically heterogeneous velocity structures, is related to contrasts of seismic impedance at depth. However, these are themselves not frequency-dependent (as ratios between locally constant elastic parameters) and are therefore difficult to correlate directly with the V/H curves. For this reason, we introduce the concept of quarter-wavelength seismic impedance contrast (IC^{qw}). Such an approach gives the possibility of directly relating the seismic velocity contrast with specific spectral ordinates.

In practice, the IC^{qw} parameter can be described as the velocity contrast obtained from the ratio between two quarter-wavelength average velocities (Fig. 1, equation 1). The top estimate corresponds to the classic travel-time velocity averaged down to a depth (Z_1) corresponding to $1/4$ of the wavelength of interest λ_1 (i.e., the classical quarter-wavelength depth). The bottom velocity estimate is obtained as the average along the velocity profile from the depth Z_1 to $Z_1 + \lambda_2/4$. λ_2 is related to λ_1 by keeping the considered frequency constant.

$$IC^{qw}(f) = \frac{V_{S1}^{qw}(f, \lambda_1/4)}{V_{S2}^{qw}(f, \lambda_2/4)} \quad (1)$$

As an illustrative example, Figure 2 presents the range of variation of the quarter-wavelength parameters (travel-time depths, average velocities and seismic impedance contrast) versus frequency, computed from the profile given in Figure 1.

In sedimentary basins with a strong velocity contrast, the IC^{qw} curve includes characteristic troughs, directly related to the most significant interfaces at depth. The first trough, when moving along the frequency axis of such a curve, can be reasonably considered as a good proxy for the fundamental frequency of resonance of the site (f_0 in Fig. 2).

The Japanese Dataset

In this study, a Japanese dataset of earthquake recordings from the dense KiK-net strong-motion network is analyzed (Aoi *et al.*, 2004). The dataset includes a collection

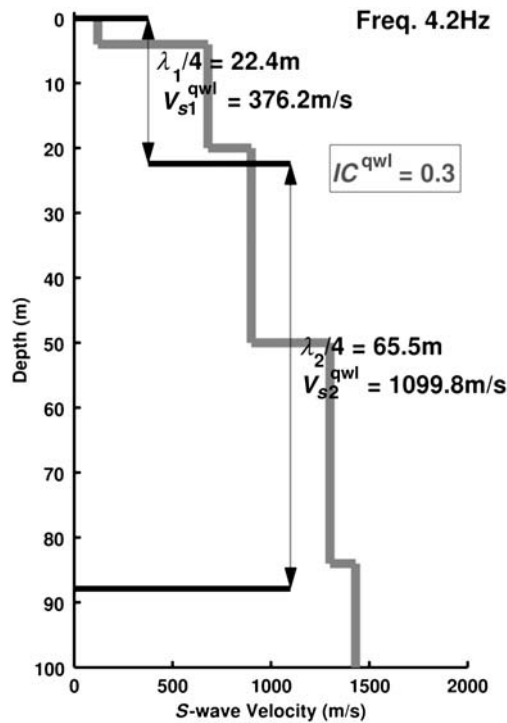


Figure 1. Example of estimation of the quarter-wavelength average velocity (V_S^{qw1}) and impedance contrast (IC^{qw1}) parameters from an S -wave velocity profile at the frequency of 4.2 Hz.

of velocity profiles (P and S) from 689 sites of the network. These profiles were provided by the Japanese National Research Institute for Earth Science and Disaster Prevention (NIED) and were obtained from downhole logging in boreholes set up for the installation of buried sensors. From the whole dataset with 689 sites, a subset of 220 sites was analyzed in this study. The sites were selected based on the comparison of the fundamental frequencies of resonance (f_0) directly estimated from the recordings and by indirect modeling methods using the velocity profile (Fig. 3). Sites where the fundamental frequencies estimated from different methods visibly mismatched (in general more than $\pm 0.5f_0$) were discarded. The selection spans a range of sites, mostly on soft sediments, with average S -wave velocity over the first 30 m (V_{S30}) between about 100 and 900 m/s (Fig. 4). In the selection, the variability of the fundamental frequency is also well represented, spanning a broad range between about 1 and 15 Hz.

A total of 12,963 records were used to compute the V/H ratio of the 5%-damped pseudo-acceleration response spectra of each of the 220 selected station locations. All stations recorded five or more events. Limits on the valid frequency range were imposed by employing signal-to-noise ratio (SNR) checks on the Fourier spectra following the method detailed in Edwards *et al.* (2010). Response spectra lower limits were defined at 1.2 times the frequency where the Fourier spectra SNR fell below 3 (Akkar *et al.*, 2006; Douglas and Boore, 2010).

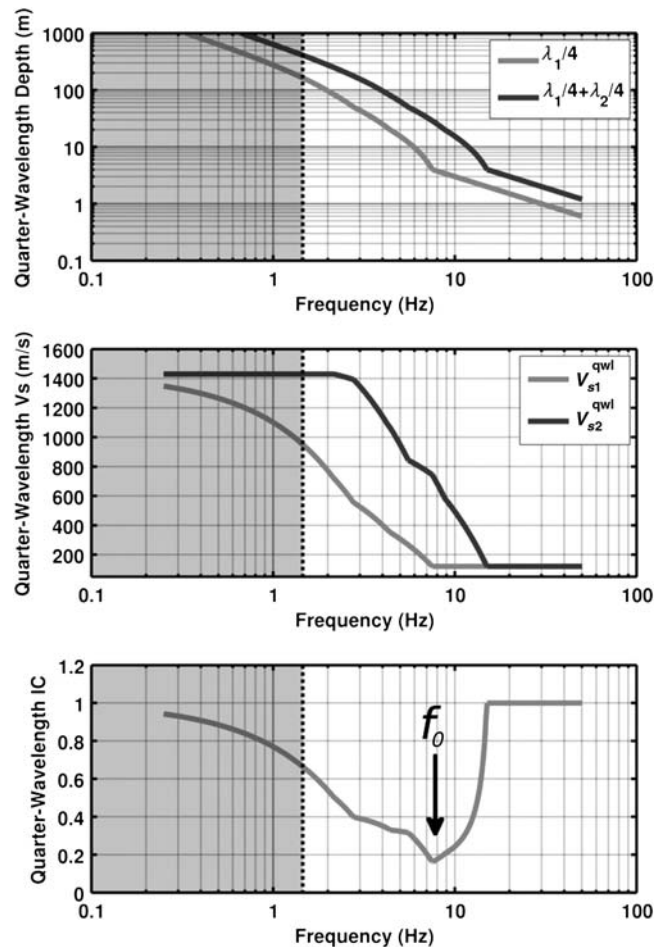


Figure 2. Quarter-wavelength depth, average velocity (V_S^{qw1}), and impedance contrast (IC^{qw1}) curves of the velocity profile presented in Figure 1. Dashed line defines the frequency region of reliability, where the curves are constrained by the measured velocity profile. The fundamental frequency of resonance (f_0) is also shown.

V/H Correlations in Three-Dimensional Space

The V/H ratios of the 5%-damped response spectra were compared with the quarter-wavelength velocity (V_S^{qw1}) and quarter-wavelength impedance contrast (IC^{qw1}) over a range of discrete frequencies between 0.5 and 20 Hz. However, due to the different resolution depths of the various KiK-net velocity profiles, the whole frequency range was not used at all sites. In practice, for a given site, the lower resolvable frequency (f^{min}) is controlled by the corresponding maximum quarter-wavelength depth that is still constrained by the profile data. Additionally, following the same procedure as in Edwards *et al.* (2011), we also allow the V_S^{qw1} and IC^{qw1} functions to be partially extrapolated using cubic interpolation down to a frequency equal to $0.5f$. This is realistic, as no large variations are expected in this range, and the average quarter-wavelength velocity estimates are still mostly constrained by the velocity profile of the upper layers. Moreover, because the velocity profile is assumed to have constant

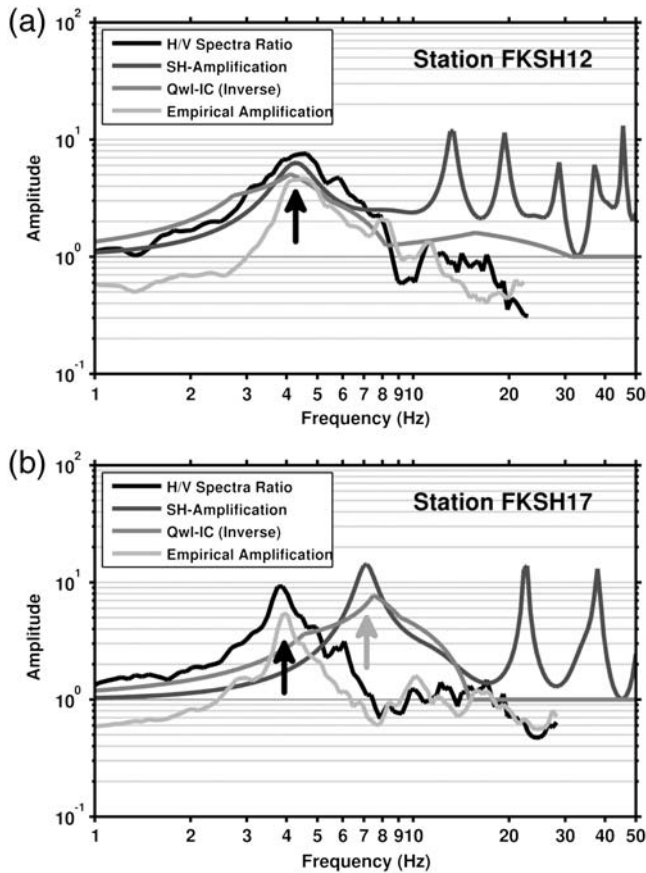


Figure 3. Japanese stations were selected by comparison of the fundamental frequency of resonance estimated from observed H/V Fourier spectra ratio, empirical modeling of earthquake spectra (Edwards *et al.*, 2008), SH-wave transfer function, and the quarter-wavelength seismic impedance contrast (IC^{qwl} , in inverse form for better comparison) derived from the velocity profile. Here, an example is given of a selected station (on top) and a rejected one (bottom). For this last, a clear mismatch between the modeled (gray arrow) and the observed (black arrow) fundamental frequency is visible.

velocity below the prescribed depth limit, the IC^{qwl} parameter is expected to asymptotically converge to the value of 1 at frequencies progressively lower than the f of the profile. In this way, the resonance information is ensured to be mapped into the prescribed reliability range.

To explain data correlation, different regression relations were tested using statistical significance tools. However, after residual analysis, the following best-fitting relation with as few parameters as possible was found:

$$\ln\left[\frac{V}{H}(f)\right] = a \cdot \ln(V_S^{qwl}) - b \cdot \exp(-IC^{qwl}) + c. \quad (2)$$

The logarithmic dependency between the V/H and V_S^{qwl} has been kept for compatibility with the previous study (Edwards *et al.*, 2011), while an exponential function is used to explain the data distribution along the IC^{qwl} axis (Fig. 5).

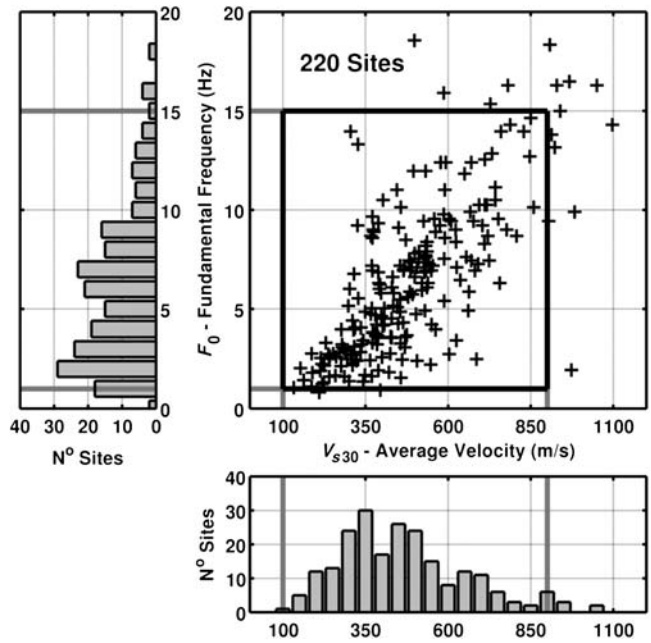


Figure 4. Distribution of the fundamental frequency of resonance (F_0) and of the average velocity over the first 30 m (V_{S30}) for the 220 selected sites of the Japanese KiK-net network. From the distribution, it is expected to have sufficient constraint on sites with V_{S30} between about 150 and 800 m/s, while fundamental frequencies are fully represented in a broad range between 1 and 15 Hz.

A simple log-linear dependence on IC^{qwl} would have indeed led to unrealistically high V/H values—which are never observed—for $IC^{qwl} \approx 1$ and rather high frequencies. On the contrary, a smooth asymptotic behavior of the $\ln(V/H)$ is observed, which tends to saturate around the value of one. Statistical significance tests (T and χ^2) on the distribution of residuals were also performed to confirm our working hypothesis. For each analyzed frequency between 0.5 and 20 Hz, the coefficients a , b , and c of the relation were obtained by minimization of the residuals between observed and predicted V/H data, using an unconstrained nonlinearized optimization procedure, also referred to as the simplex search method of Lagarias *et al.* (1998). As starting model, coefficients a and c were imposed to be consistent with those from Edwards *et al.* (2011), while the b parameter was initially set to 0. An example of the result is given in Figure 5, while the whole set of coefficients versus frequency can be found in Table 1. It must be noted that the regression predictors V_S^{qwl} and IC^{qwl} appear to be affected by a form of dependency. However, in reality there only exists a conditionality constraint in the distribution of the IC^{qwl} parameter space (V_{S2}^{qwl} realizations are not affected by V_{S1}^{qwl}). As verified through synthetic testing, this conditionality does not affect the robustness of the regression with the V/H ratios, as long as the sampling of the parameter space is sufficient.

Comparing the regression results over the whole analyzed frequency range (Fig. 6) shows a small trend with frequency, which is more evident with IC^{qwl} (parameter b in

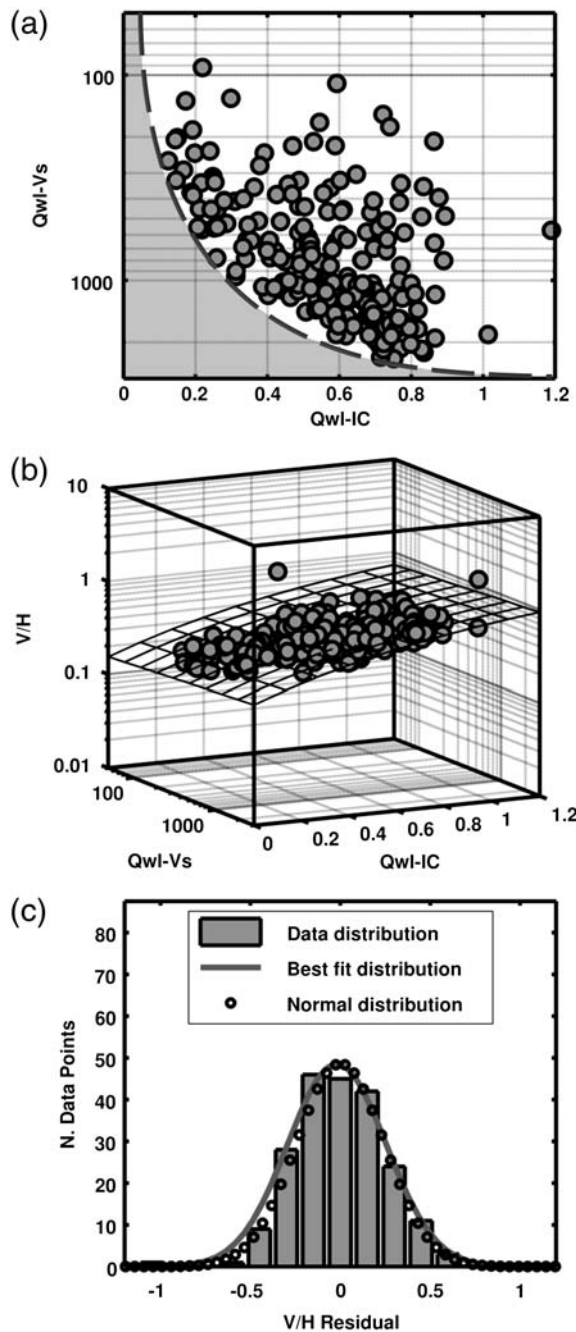


Figure 5. Correlation between the V/H ratio of the average response spectra, the 1/4 wavelength V_S (V_S^{qwl}) and the 1/4 wavelength IC (IC^{qwl}) parameters. For the regression, the 220 selected sites of the Japanese network were used. Each dot corresponds to one site. The plots are for a frequency of 2.0 Hz in this example. In (a) the distribution of data in the $IC^{qwl}-V_S^{qwl}$ parameter space are shown; the gray region indicates the physical limit of IC^{qwl} , given V_S^{qwl} . In (b) the three-dimensional regression function is given. In (c) the distribution of residuals (log) between observations and prediction at this frequency is provided.

Table 1) and at high frequencies. However, due to the limited resolution of the profiles at shallow depth, correlations at frequencies higher than about 10 Hz were considered less stable and only carefully used further on. Although this limits the

Table 1
Coefficients of the Regression in the Frequency Range 0.5–20 Hz

Frequency (Hz)	<i>a</i>	<i>b</i>	<i>c</i>	σ
0.5	0.1978	2.9084	-0.4840	1.3482
1.0	0.0547	2.0526	0.0572	1.2808
2.0	0.0590	2.2341	0.1362	1.2782
3.0	0.0964	2.0441	-0.2041	1.3170
4.0	0.1056	1.9266	-0.3186	1.3465
5.0	0.1115	1.8064	-0.4436	1.4040
6.0	0.0663	1.9083	-0.1238	1.4252
7.0	0.0556	1.8875	-0.0780	1.4240
8.0	0.0462	1.8156	-0.0651	1.4316
9.0	0.0020	1.7706	0.1818	1.4608
10.0	-0.0574	1.5746	0.4256	1.4774
15.0	-0.2851	1.3405	1.7393	1.4485
20.0	-0.1145	0.8356	0.7287	1.4099

Last column shows the computed standard deviations (in log-statistic).

determination of V/H through such correlations up to frequencies commonly used in engineering practice, we extend the prediction through to 100 Hz (PGA) through empirical corrections, discussed later.

Frequency-Independent Correlation

Comparison of the regression results in the range between 1 and 10 Hz suggests that a unique frequency-independent model of the regression coefficients *a*, *b*, and *c* can be assumed to simplify the relation between V/H, V_S^{qwl} , and IC^{qwl} in the Japanese dataset. Even if the frequency-dependent models better explain the data, the uncertainty range of each distribution make the definition of a unique

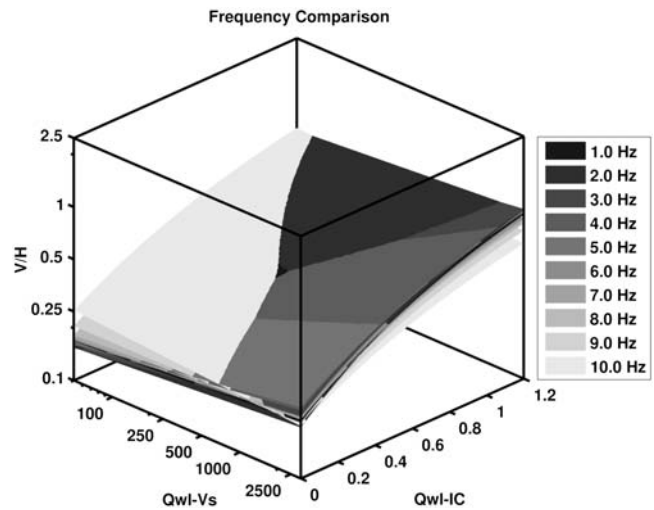


Figure 6. Comparison of the regression results between V/H ratio of response spectra, 1/4 wavelength V_S (V_S^{qwl} in m/s) and 1/4 wavelength IC (IC^{qwl}) of the Japanese dataset in the frequency range between 1 and 10 Hz. These planes are directly constrained by data in the range of about 100–1500 m/s for the V_S^{qwl} parameter and 0.2–1 for IC^{qwl} .

average model possible (see Table 1). Within the resulting uncertainties, this simplified model fits the data equally well in the studied frequency range of 1–10 Hz (Fig. 7b). Moreover, such a model has the advantage that it is also easy to implement, because a unique set of frequency-independent coefficients can be provided instead of a set of values for each discrete frequency. Furthermore, problems related to the interpolation between discrete frequencies can also be avoided in this way. The coefficients of the frequency-independent model are given in Table 2.

It must be noted that, because the frequency-independent correlation used all available data points simultaneously, the sigma from this regression is therefore more heavily influenced by data in the range 3–7 Hz, where the larger amount of data is available. The frequency-independent correlation therefore shows a corresponding sigma value to the frequency-independent regressions in the range 3–7 Hz.

Back-Reconstruction of the V/H Ratio at Test Sites

Coefficients from the previously defined frequency-dependent and the frequency-independent correlations were used to back-reconstruct the V/H ratio at specific test sites of the Japanese network (Figs. 8 and 9). For each specific station location, the V/H functions were computed down to a frequency corresponding to the resolved part of the velocity profile. The curves were then compared with observed V/H to assess the robustness of the performed regression. For most of the tested sites, a good match was found, as the method also provides the possibility of reconstructing complex features of the curve, such as strong V/H minima induced by resonance effects. In some cases, small discrepancies were present, probably related to some oversimplification of the V_S profile at the corresponding station location. In comparison, the use of frequency-dependent or frequency-independent correlations produces similar results in the whole frequency range between 1 and 10 Hz (Fig. 10a). As expected, however, at higher frequencies (> 10 Hz) some deviations are progressively observable. In this band, the frequency-independent result gradually deviates from the observation (see as an example station KSRH06 in Fig. 9), as the coefficients no longer represent a good correlation with data. A possible reason might be the limited resolution of the velocity profiles in the shallow part of the soil structure. It is nevertheless possible to map the average trend of the difference in V/H between frequency-dependent and -independent correlation models (as for the mean curve in Fig. 10a). In this way, we can define a simple correction function which can be used to partially compensate for the deviations observed in this frequency range (e.g., in Fig. 10b). For all these reasons, the frequency-independent model has been identified as the preferred model and will be used later on for the analysis of the model dependence on magnitude–distance and for the disaggregation of the total sigma into between- and within-event uncertainty.

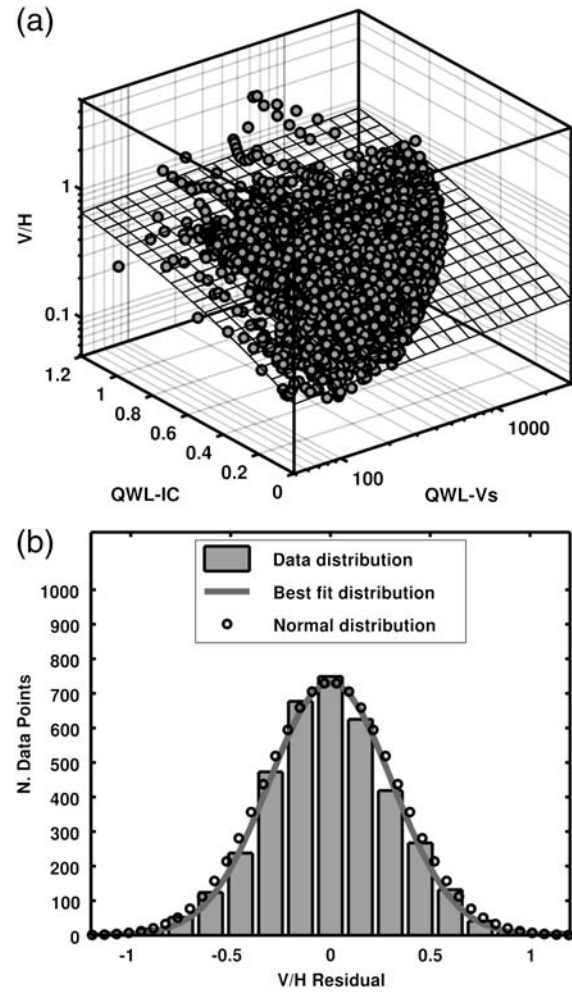


Figure 7. (a) Frequency-independent regression obtained from simultaneously fitting all frequencies in the range 1–10 Hz. (b) Residual distribution of the frequency-independent regression; (log) residuals are normally distributed around the regression plane.

Comparison Between Methods

As already highlighted, the proposed method for computing V/H ratios of response spectra has to be considered an extension of the approach presented in Edwards *et al.* (2011) in the case of soft sediments and resonance phenomena. Because of the distribution of sites used for calibration, a range of applicability of V_{S30} velocities between about 150 and 800 m/s was established for the proposed method, while for the former the authors proposed the applicability for sites

Table 2
Coefficients of the Frequency-Independent Correlation

a	b	c	σ
0.0646	1.9099	-0.0902	1.3932

Last column shows the computed standard deviations (in log-statistic).

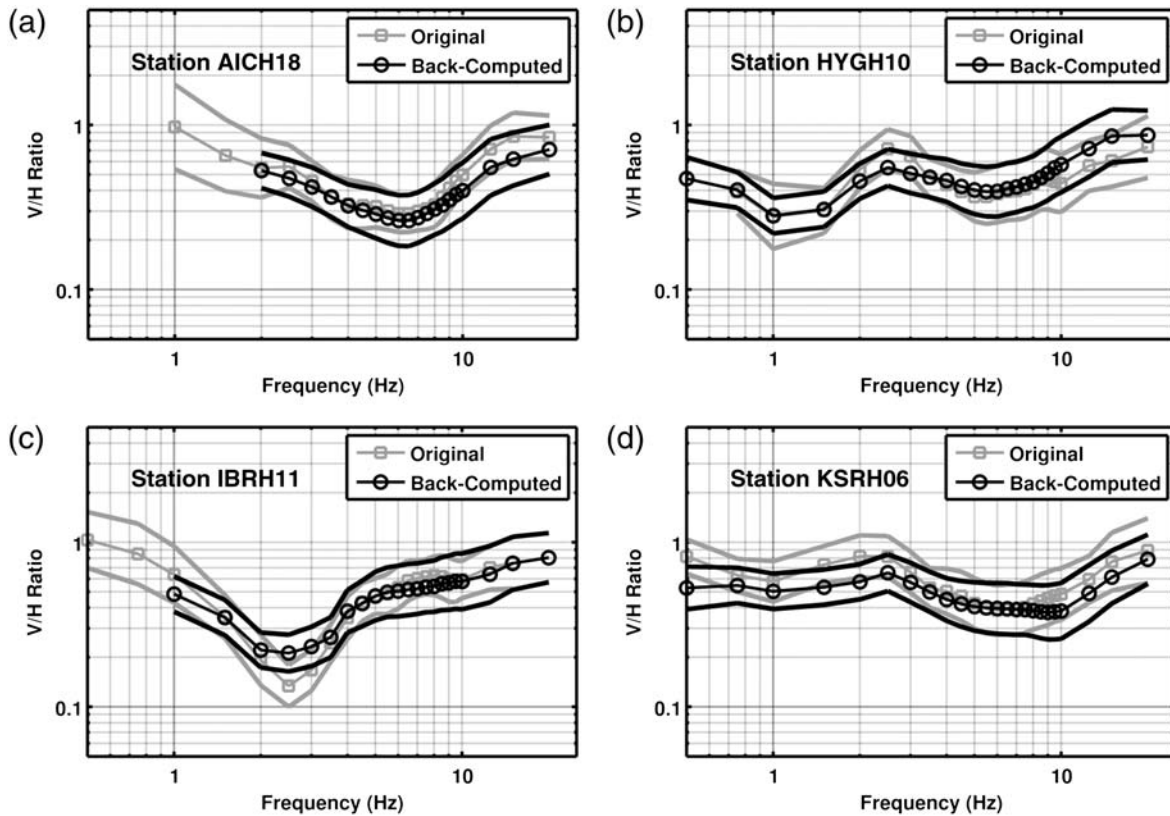


Figure 8. Back-computation of the V/H response spectra ratio at four KiK-net stations using the coefficients from the frequency-dependent correlations. Mean and mean \pm standard deviation are given. (a) $V_{S30} = 499$ m/s, (b) $V_{S30} = 223$ m/s, (c) $V_{S30} = 242$ m/s, (d) $V_{S30} = 326$ m/s.

with average velocity higher than 800 m/s at the surface. As the methods are to a certain extent complementary, we want to ensure that they produce compatible results in the vicinity of their separation boundary. For this reason, we tested a subset of 22 of the 220 KiK-net sites with V_{S30} velocity between 700 and 900 m/s. For all these sites, the V/H ratios have been modeled using both methods and then compared to the measured values (Fig. 11). The analysis showed a clear agreement between the two approaches in this range of soil velocity. This was nevertheless expected, as at stiff sites with rather high velocity, the effect of IC^{qwl} in equation (2) becomes progressively negligible while increasing the fundamental frequency of resonance ($f_0 > 8$ Hz in the examples given in Fig. 11).

Model Dependence on Distance and Magnitude

So far, we have analyzed V/H ratios solely in terms of site averages and physical site properties. The presented correlations were shown to successfully reconstruct this site-specific average V/H function. However, for the purpose of engineering or hazard application, the V/H ratio must be presented in a way that is useful and, preferably, easy to implement. A key requirement of such an application is the availability of V/H ratio through a range of periods of engineering interest, typically around 2–0.01 s. Furthermore,

previous authors (e.g., Bommer *et al.*, 2011; Edwards *et al.*, 2011; Gülerce and Abrahamson, 2011) have shown that the V/H ratio is dependent on distance, and in some cases, on magnitude. This is a particularly important feature to consider in terms of correcting CMS. In order to approach this issue, the computed record-specific V/H response spectral-ratios are used to extend the prediction to high frequencies (100 Hz, PGA) and statistically analyze the magnitude–distance dependency of the derived correlations. We account for the inclusion of high-frequency ($f > 10$ Hz) predictions of V/H and the possibility of V/H being dependent on distance and magnitude through regression of the residual misfit to the frequency-independent $V_S^{qwl} - IC^{qwl} - V/H$ model. This has the advantage that we build on the simple basis model for predicting the average site-specific V/H from frequency-independent correlations, while the frequency–distance–magnitude correction can incorporate both the adjustment to the frequency-dependent correlations, in addition to any frequency-dependent distance–magnitude specific features. In a first step we solve the following functional form at log-spaced discrete frequencies (0.5–100 Hz):

$$\begin{aligned} \delta(M, R, f) &= \ln \left[\frac{(V/H)_{\text{Obs}}}{(V/H)_{\text{Mod}}} \right] (f) \\ &= d_1(f) + d_2(f)M_{\text{JMA}} + d_3(f) \ln(R_{\text{hyp}}), \quad (3) \end{aligned}$$

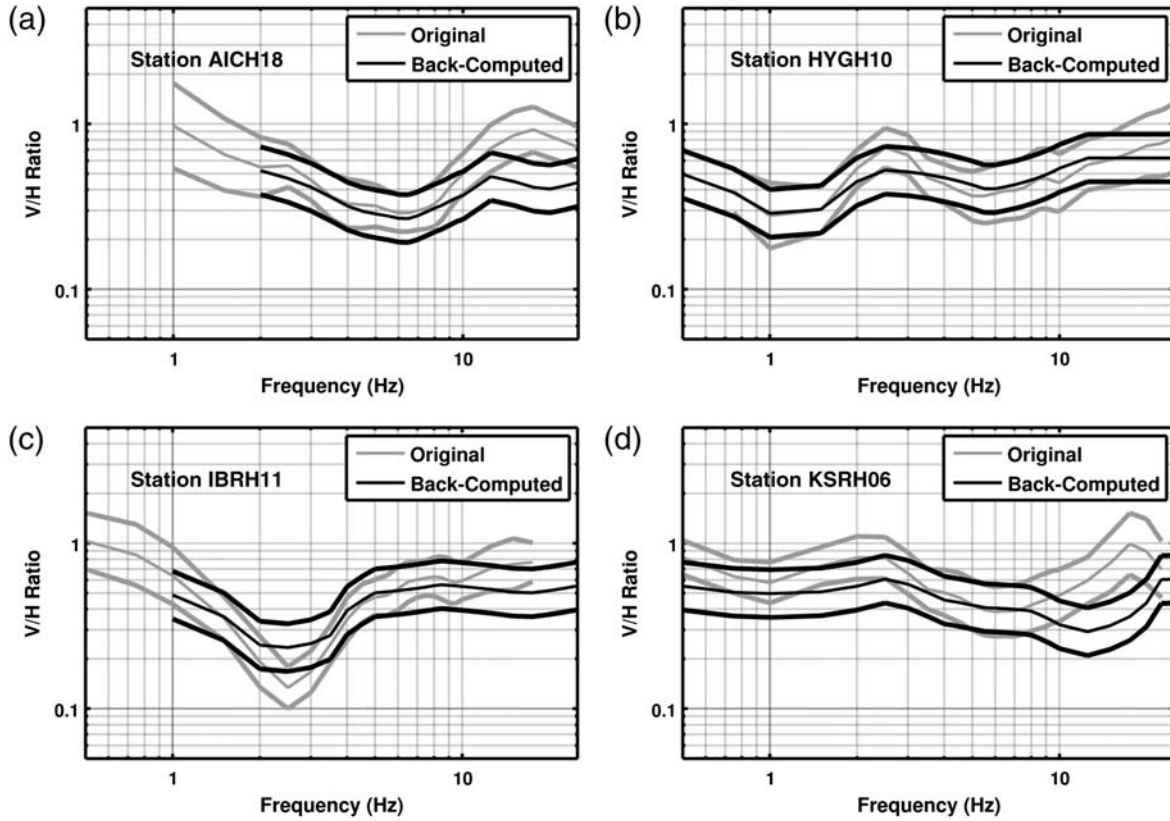


Figure 9. Back-computation of the V/H response spectra ratio at four KiK-net stations using the coefficients from the frequency-independent correlation. With respect to the V/H ratios computed using the frequency-dependent coefficients (Fig. 8) some deviations are observed at high frequencies. (a) $V_{S30} = 499$ m/s, (b) $V_{S30} = 223$ m/s, (c) $V_{S30} = 242$ m/s, (d) $V_{S30} = 326$ m/s.

d_1 accounts for the difference between the frequency-independent and dependent $V_S^{\text{qwl}}-IC^{\text{qwl}}-V/H$ correlations (extending the validity of the frequency-independent model above 10 Hz), in addition to accommodating the intercept of the magnitude and distance corrections. One may question the use of frequency-independent $V_S^{\text{qwl}}-IC^{\text{qwl}}-V/H$ correlation, if we then re-introduce the frequency dependence through the use of the d_1 parameter here. The answer is that we can now describe this frequency dependence using a simple functional form. It should also be noted that d_1 is not necessarily equal to unity between 1 and 10 Hz due to the inclusion of the distance and magnitude corrections.

Only $M_w \geq 4.0$ are used in order to avoid using records that may be biased due to the selective triggering of the instrumentation. Furthermore, the limiting low-frequency resolution at each site is defined by the maximum profile depth threshold defined earlier. Values for parameters d_1 , d_2 , and d_3 are shown in Figure 12 and Table 3.

At lower frequencies ($f < 2$ Hz) the data available for regression is limited due to the depth of the velocity profiles being insufficient to provide a $\frac{1}{4}$ wavelength velocity. This results in poorly constrained regressions and scattered values of the coefficients at low frequency. To provide a more robust result we impose a functional form to the coefficients based on data distribution of Figure 12:

$$d_1 = \frac{1}{1 + \left(\frac{f}{e_0}\right)^8} \ln \left[\frac{\exp(e_1 f)}{e_2 + e_3 \exp(e_4 f)} + e_5 \right] \quad d_2 = 0$$

$$d_3 = \frac{1}{1 + \left(\frac{f}{e_0}\right)^8} [e_6 + \exp(e_7 f)] + e_8. \quad (4)$$

$d_2 = 0$ imposes magnitude independence on the V/H equation, which is justified when seeing that for the regressions for a discrete frequency, the maximum value of d_2 was much smaller than the other coefficients. This is also consistent with the observations of [Bommer et al. \(2011\)](#) who found only insignificant dependence of V/H on magnitude.

A non-linear least-squares regression for parameters e_0 to e_8 was carried out, using a starting model based on the preliminary fit to the frequency-dependent d_1 and d_3 coefficients. The resulting values are given in Table 4. The result of the correction can be seen in Figures 13 and 14. From Figure 13, a different behavior of the distance dependency at high and low frequency is evident. In general, the near field (roughly < 30 km) introduces larger deviation at rather high frequencies, while in the far field the influence of long wavelengths is more pronounced. This is in agreement with the standard model, where a higher contribution of body

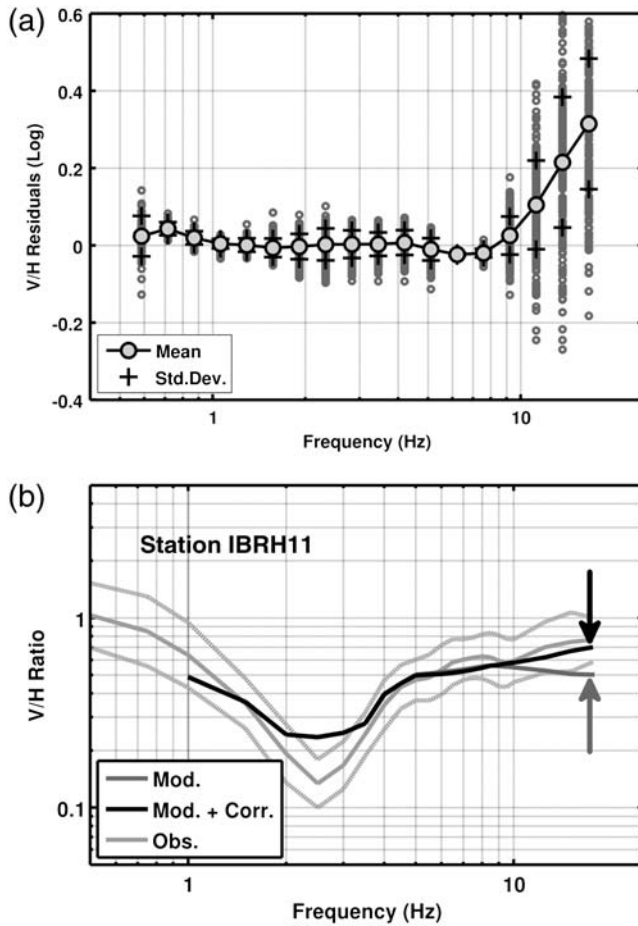


Figure 10. (a) Distribution over frequency of the logarithmic differences between V/H response spectral ratios computed from the frequency-dependent and the frequency-independent relations. Mean and standard deviation of the distribution are also presented. No significant deviations are observable below about 10 Hz. (b) Example of correcting the high frequencies of a V/H function from frequency-independent coefficients by using the average residual function in (a).

waves is expected close to the source, which are conversely more attenuated at far distances, where long-period surface waves become progressively dominant. Nevertheless, only in the nearest 50 km to the source is any significant correction applied (considering the total uncertainty).

Residual misfit was computed after accounting for the V_S^{qw1} - IC^{qw1} -V/H model and the correction given in equations (3) and (4). No remaining residual dependence on magnitude, distance, or frequency was apparent (Fig. 15). This relation is valid for a hypocentral distance range between 2 and 200 km, and a frequency range between 0.5 Hz and PGA.

Uncertainty

Assuming normal statistics, the total uncertainty of the V/H model (from the frequency-independent correlation coefficients) is given by

$$\sigma^2 = \frac{1}{N} \sum_{n=1}^N \{Y_n - \ln[f_n(\mathbf{X}_{es}, \Theta)]\}^2 \quad (5)$$

(Al Atik *et al.*, 2010), where Y_n is the natural log of the V/H ratio and $f_n(\mathbf{X}_{es}, \Theta)$ is that predicted by the model at a given frequency for observation n . \mathbf{X}_{es} is the vector of independent parameters (in this case the frequency and corresponding $\frac{1}{4}$ wavelength velocity and distance), and Θ is the vector of model parameters (the coefficients of the regressions). This can be split into between- (inter) and within- (intra) event terms, τ and ϕ , respectively:

$$\sigma = \sqrt{\tau^2 + \phi_{ss}^2 + \phi_{s2s}^2} \quad (6)$$

with the within-event term ϕ defined by between- and within-site terms, ϕ_{s2s} and ϕ_{ss} respectively.

This formulation is very useful for site-specific hazard analyses, where the so-called single-site sigma is more representative of variability at the site, as it removes the contribution to uncertainty by using numerous sites in the derivation of models:

$$\sigma_{ss} = \sqrt{\tau^2 + \phi_{ss}^2} \quad (7)$$

Sigma values are presented in Table 5 for different frequencies and distance ranges. In general, the lower the frequency of interest, the lower the uncertainty, with sigma values peaking at around 20 Hz. This is likely to be due to the lower sensitivity of long periods with respect to small-scale heterogeneities in the soil structure, or alternatively to the limited resolution (and therefore predictive power) of the available velocity profiles at shallower depths. The main difference in uncertainty in terms of distance is seen in the τ value (between-event uncertainty). τ is higher for smaller distances from the source, indicating the increased complexity of wave propagation in the near field. The within site term, ϕ_{ss} , dominates the total V/H uncertainty, while σ_{ss} is systematically reduced relative to total sigma, due to the removal of the between-site term, ϕ_{s2s} . Table 6 shows correction factors (ν) to the uncertainty values for specific magnitude ranges relative to the values in Table 5. These factors can be multiplied with the uncertainty values taken from Table 5 to obtain magnitude-specific uncertainty. For instance, assuming an event with M 6.5 at distance 30 km, we could take the value $\sigma(\text{PGA}) = 0.478$ (Table 5, M 4.5–7.3; R0-50 km). This represents the average value over magnitudes 4.5–7.3. For a magnitude-specific value, we then refer to Table 6. For example, for M 6–7.3, the correction factor is $\nu_\sigma(0.5 \text{ Hz}) = 0.958$; hence $\sigma(\text{PGA}, M6.5) = 0.478 \times 0.958 = 0.458$. It can be observed that sigma is significantly lower for higher magnitude events. This difference is almost entirely due to the between-event parameter, τ , which is over a factor of two higher for M 2–3 than M 6–7.3; nevertheless, it should be noted that the model was derived for magnitudes greater than four. The source

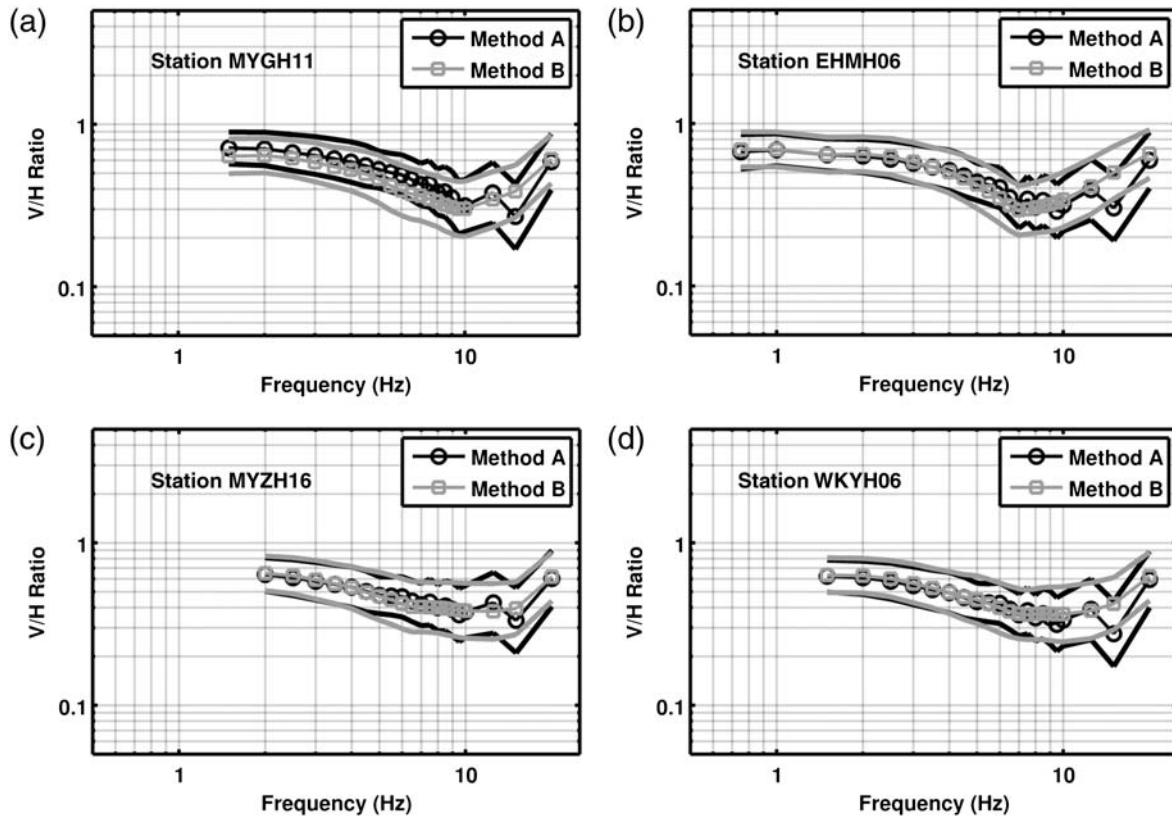


Figure 11. Comparison between back-computed V/H ratios from the method for rock sites in [Edwards *et al.* \(2011\)](#), indicated as method A in the legend, and the proposed (method B). The comparison is made for those sites of the KiK-net selection with V_{S30} between about 700 and 900 m/s, therefore in the overlapping region of applicability of the two approaches. The comparison of 4 out of 22 stations is presented here. (a) $V_{S30} = 859$ m/s, (b) $V_{S30} = 717$ m/s, (c) $V_{S30} = 847$ m/s, (d) $V_{S30} = 752$ m/s.

component of variability of V/H for small earthquakes is therefore significantly higher than for large events.

Testing of the Method for Soft-Sediment Sites in Switzerland

The method has been tested on three permanent station locations (SBAF; SMZW; ZUR; Fig. 16) of the Swiss Digital Seismic Network (SDSNet, [Deichmann *et al.*, 2010](#)) and the Swiss Strong Motion Network (SSMNet). An additional station from a temporary seismic network in Visp (VISP2)

investigated within the COGEAR project (Coupled seismo-genic Geohazards in Alpine Regions, [Fäh *et al.*, 2012](#)) was also analyzed. For each station, a shear-wave velocity profile is available from the site-characterization database of the Swiss Seismological Service (SED), derived from surface-wave dispersion analysis of non-intrusive ambient vibration recordings ([Havenith *et al.*, 2007](#); [Fäh *et al.*, 2009](#)). The three-component high-resolution f - k method ([Fäh *et al.*, 2008](#); [Poggi and Fäh, 2010](#)) was used to analyze phase velocity dispersion. Profiles are reliable down to a depth of about 100–150 m, according to resolution limits of the

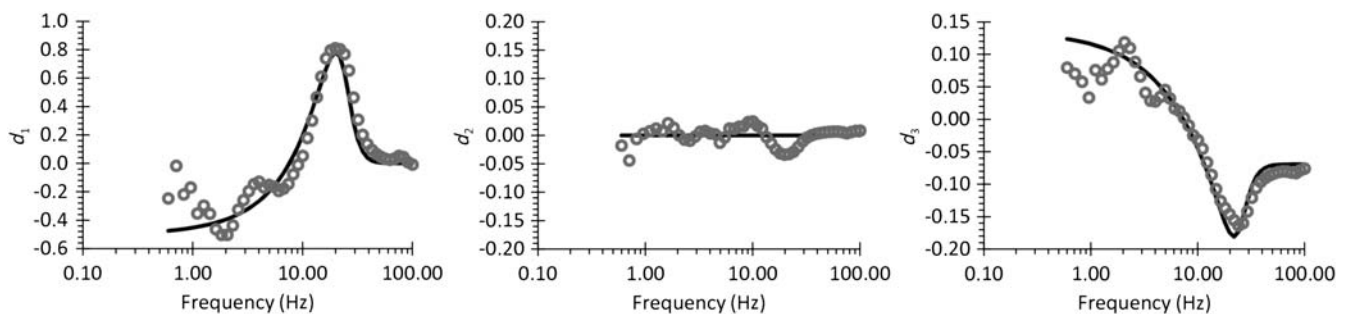


Figure 12. Parameter values d_1 , d_2 , and d_3 from equation (3). Circles: for discrete frequency regressions (Table 3). Black line: functional form constrained values (equation 4, Table 4).

Table 3
Parameter Values d_1 , d_2 , and d_3
from Equation (3)

Frequency (Hz)	d_1	d_2	d_3
0.60	-0.24630	-0.01770	0.07978
0.83	-0.21784	-0.00608	0.05795
1.10	-0.35215	0.00757	0.07601
1.43	-0.35433	0.00773	0.07801
1.83	-0.50265	0.01364	0.10574
2.31	-0.43610	-0.00732	0.11009
2.90	-0.25811	-0.00186	0.06629
3.60	-0.14597	0.00813	0.02874
4.45	-0.16914	0.00214	0.03484
5.48	-0.16275	-0.00332	0.03243
6.71	-0.17699	0.01183	0.01290
8.21	-0.07631	0.01629	-0.00934
10.01	0.05344	0.02477	-0.03160
12.18	0.30166	0.01219	-0.06623
14.81	0.61139	-0.01353	-0.10733
17.98	0.79746	-0.03137	-0.13662
21.80	0.80521	-0.03269	-0.15526
26.42	0.65502	-0.02018	-0.15988
32.00	0.30824	-0.00371	-0.12073
38.72	0.13695	0.00293	-0.09629
46.85	0.06720	0.00562	-0.08629
56.65	0.03259	0.00687	-0.08124
68.48	0.03429	0.00575	-0.08038
82.76	0.04490	0.00618	-0.08282
100.00	-0.00778	0.00855	-0.07574

method. The observed V/H ratios were obtained by using small magnitude events ($2 < M_w < 4.5$) with hypocentral distance between 2 and 200 km.

As in the previous comparison, the back-computed V/H curves obtained using the originally frequency-independent coefficients are in agreement with local observations (Fig. 17). Some deviations can be observed at high frequencies (e.g., SMZW), which are probably due to a lack of resolution of the velocity profile in the first few meters. The computed V/H for station location VISIP2 is able to predict the correct shape of the measured response spectral ratio, but systematically underestimates by a factor 0.7. This is probably induced by the peculiar characteristics of the underlying sedimentary basin, which is typically V-shaped—as in most alpine valleys—and with high shape ratio (Bard and Bouchon, 1985). In such a case, the effect of possible 2D resonances and of edge-generated surface waves is significant (Roten et al., 2008), which may explain then the discrepancies between modeled V/H ratios and observation. Moreover, we have not identified such behavior in the V/H at Japanese

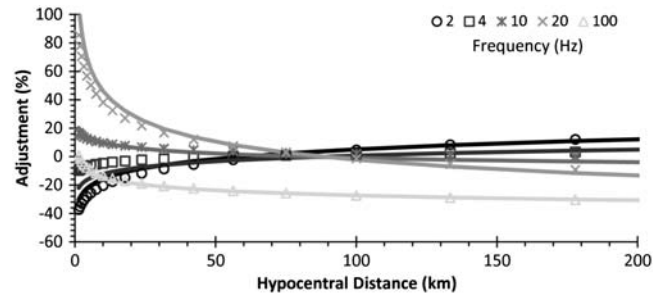


Figure 13. Correction of $V_S^{qwl}-IC^{qwl}-V/H$ model for an M_w 4.5 event at various distances. Symbols indicate the correction obtained for the individual frequency regression of $d_1(f)$, $d_2(f)$, and $d_3(f)$, whereas the lines show the correction using parameters e_1-e_7 .

sites, probably because of the absence of a similar environment in the selected KiK-net stations.

For the station SBAF, finally, a comparison between V/H spectral ratios computed using the proposed frequency-independent correlations and from a selection of independent methods available in literature is presented in Figure 18. The prediction is consistent between the different models, with the exception of Campbell and Bozorgnia (2003), which appears to slightly overestimate the ratio in the low-frequency range by a factor of approximately 1.5~2. It has to be noticed that the shape of the V/H curves from these models are rather different from the site-specific, due to the use of the V_{S30} parameter, which is not sufficient to map the variability of the resonance trough location.

Conclusions

An extension of the method proposed by Edwards et al. (2011) to compute the V/H ratio of 5%-damped response spectra for soft-sediment sites has been proposed. The method makes use of the quarter-wavelength parameters (IC^{qwl} and V_S^{qwl}) to link the local velocity structure at the site with the ground-motion estimates at the surface. The resulting V/H spectra are reliable in the frequency range of 0.5 Hz to PGA, independently from magnitude. Dependency on hypocentral distance was calibrated between 2 and 200 km. Computation of the IC^{qwl} parameter, in particular, has been demonstrated to be a powerful tool to assess the influence of resonance phenomena on the V/H ratios. As an important outcome, we confirmed that the shape of the V/H functions is mainly controlled by local site characteristics, and less evidently by the source-path related parameters. In practice, from the analysis, it was observed that only a small dependence on distance was present, while the magnitude showed

Table 4
Parameter Values for Equation (4)

e_0	e_1	e_2	e_3	e_4	e_5	e_6	e_7	e_8
25.18440	0.00227	0.31409	4.63487	-0.15961	0.40109	-0.79489	-0.01992	-0.06925

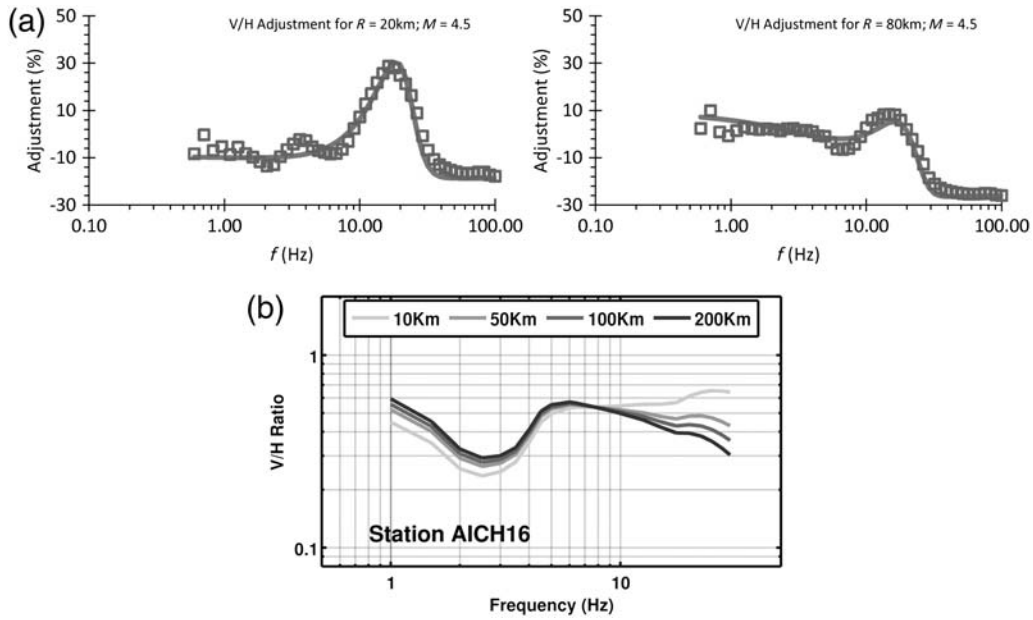


Figure 14. (a) Correction of $V_S^{\text{qw1}}-IC^{\text{qw1}}-V/H$ model for an M_w 4.5 event at 20 km (on the left) and 80 km (on the right). Squares indicate the correction obtained for the individual frequency regression of $d_1(f)$, $d_2(f)$, and $d_3(f)$, whereas the lines show the correction using parameters e_0-e_8 . (b) Example of applying the correction functions for a range of distances (10, 50, 100, and 200 km) to the computed V/H spectral ratio of a Japanese station.

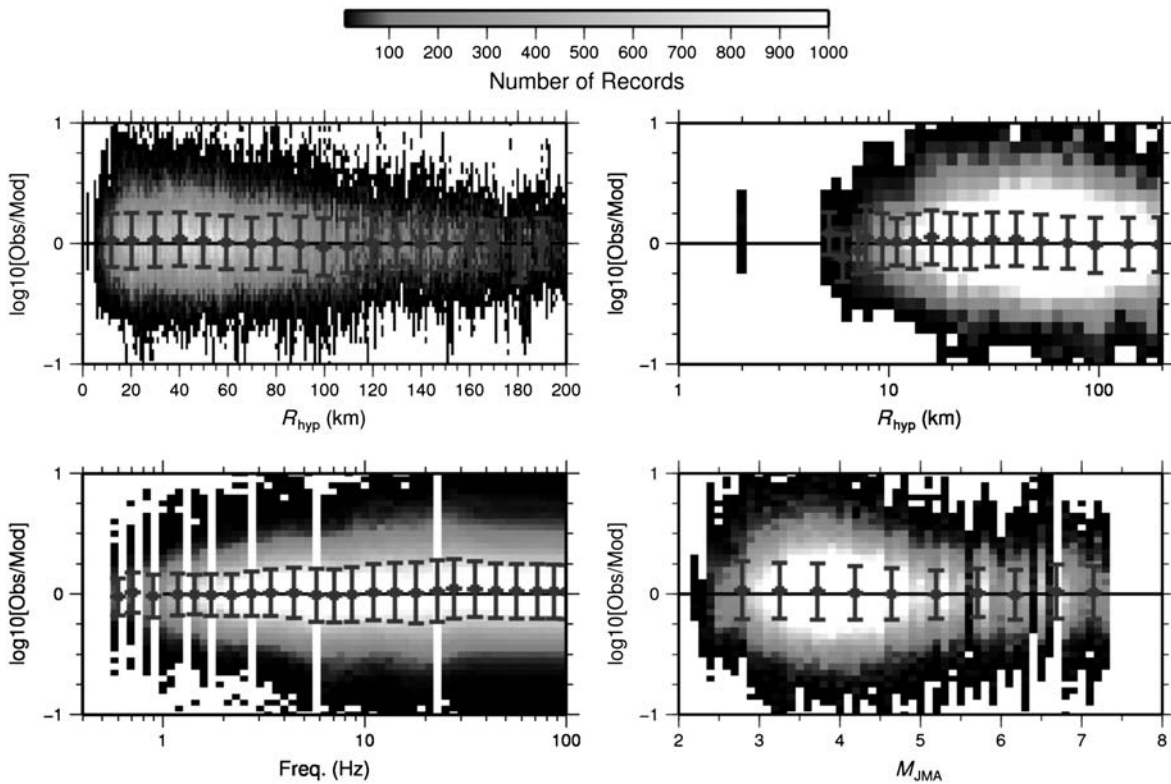


Figure 15. Residual misfit after application of the frequency-independent $V_S^{\text{qw1}}-IC^{\text{qw1}}-V/H$ model and the correction given in equations (3) and (4). The error bars indicate the mean and one standard deviation of the residuals.

Table 5
Sigma Values (Natural-Log Units) Separated into Source and Site Contributions for Given Magnitude Range (*M*) and Different Hypocentral Distance Ranges (*R*)

f (Hz)	<i>M</i> = 4.5–7.3, <i>R</i> = 0–200					<i>M</i> = 4.5–7.3, <i>R</i> = 50–100					<i>M</i> = 4.5–7.3, <i>R</i> = 100–200									
	σ	τ	ϕ_{SS}	ϕ_{SS}	σ_{SS}	σ	τ	ϕ_{SS}	ϕ_{SS}	σ_{SS}	σ	τ	ϕ_{SS}	ϕ_{SS}	σ_{SS}					
0.83	0.397	0.177	0.229	0.271	0.324	—	—	—	—	—	0.415	0.206	0.234	0.274	—	0.385	0.155	0.232	0.264	0.307
1.10	0.431	0.168	0.262	0.297	0.341	—	—	—	—	—	0.425	0.209	0.250	0.272	0.343	0.439	0.200	0.249	0.301	0.361
1.43	0.410	0.158	0.244	0.289	0.329	—	—	—	—	—	0.422	0.186	0.266	0.271	0.328	0.402	0.153	0.264	0.281	0.320
1.83	0.410	0.143	0.244	0.297	0.330	0.393	0.252	0.160	0.256	0.359	0.427	0.165	0.262	0.294	0.337	0.404	0.122	0.255	0.286	0.311
2.31	0.412	0.129	0.244	0.305	0.331	0.462	0.223	0.228	0.335	0.402	0.421	0.154	0.257	0.295	0.333	0.421	0.133	0.267	0.296	0.324
2.90	0.416	0.117	0.260	0.303	0.325	0.451	0.185	0.276	0.304	0.356	0.436	0.148	0.297	0.284	0.320	0.434	0.137	0.288	0.295	0.325
3.60	0.431	0.121	0.284	0.301	0.325	0.441	0.196	0.284	0.275	0.338	0.436	0.148	0.297	0.284	0.320	0.434	0.137	0.288	0.295	0.325
4.45	0.459	0.151	0.316	0.297	0.334	0.465	0.214	0.301	0.284	0.355	0.451	0.176	0.325	0.260	0.314	0.464	0.163	0.336	0.276	0.321
5.48	0.488	0.152	0.353	0.300	0.336	0.449	0.172	0.282	0.304	0.349	0.477	0.172	0.344	0.282	0.330	0.495	0.175	0.380	0.264	0.317
6.71	0.490	0.157	0.349	0.306	0.344	0.514	0.162	0.331	0.359	0.394	0.494	0.173	0.374	0.272	0.323	0.495	0.181	0.365	0.280	0.334
8.21	0.477	0.146	0.333	0.309	0.342	0.530	0.196	0.365	0.331	0.384	0.482	0.154	0.369	0.269	0.310	0.452	0.172	0.296	0.294	0.341
10.01	0.499	0.151	0.344	0.328	0.361	0.548	0.208	0.382	0.334	0.393	0.535	0.174	0.417	0.287	0.336	0.472	0.194	0.306	0.302	0.360
12.18	0.520	0.183	0.332	0.356	0.400	0.541	0.220	0.369	0.328	0.395	0.530	0.197	0.381	0.312	0.369	0.522	0.236	0.330	0.329	0.405
14.81	0.540	0.215	0.317	0.380	0.437	0.547	0.221	0.324	0.381	0.440	0.535	0.240	0.344	0.332	0.410	0.532	0.242	0.329	0.341	0.418
17.98	0.550	0.219	0.318	0.392	0.449	0.551	0.247	0.283	0.403	0.473	0.554	0.256	0.333	0.360	0.442	0.531	0.226	0.344	0.336	0.405
21.80	0.544	0.209	0.324	0.384	0.437	0.564	0.268	0.302	0.394	0.476	0.552	0.254	0.339	0.353	0.435	0.525	0.207	0.354	0.328	0.388
26.42	0.520	0.193	0.304	0.375	0.422	0.567	0.299	0.269	0.400	0.499	0.519	0.246	0.311	0.336	0.416	0.495	0.189	0.334	0.313	0.366
32.00	0.483	0.165	0.294	0.346	0.383	0.521	0.229	0.303	0.357	0.424	0.465	0.212	0.290	0.290	0.363	0.477	0.181	0.323	0.300	0.351
38.72	0.474	0.158	0.296	0.335	0.370	0.492	0.198	0.307	0.329	0.384	0.452	0.204	0.290	0.281	0.347	0.475	0.181	0.325	0.296	0.347
46.85	0.471	0.156	0.297	0.331	0.365	0.482	0.186	0.308	0.320	0.370	0.448	0.200	0.291	0.277	0.341	0.475	0.181	0.326	0.295	0.346
56.65	0.470	0.155	0.298	0.329	0.363	0.478	0.181	0.310	0.316	0.364	0.447	0.198	0.291	0.275	0.339	0.475	0.182	0.327	0.294	0.346
68.48	0.469	0.154	0.298	0.328	0.362	0.479	0.181	0.310	0.317	0.365	0.446	0.198	0.291	0.274	0.338	0.476	0.182	0.327	0.294	0.345
82.76	0.469	0.155	0.297	0.328	0.363	0.487	0.186	0.313	0.324	0.373	0.446	0.200	0.289	0.275	0.340	0.474	0.181	0.325	0.294	0.346
100.0	0.469	0.153	0.299	0.326	0.361	0.478	0.176	0.315	0.313	0.359	0.445	0.197	0.292	0.272	0.336	0.476	0.181	0.328	0.294	0.345

Table 6
Correction Factors (ν) of the Sigma Values for
Specific Magnitude Ranges (M)

M	0–200 km				
	ν_σ	ν_τ	$\nu_{\phi_{SS}}$	$\nu_{\phi_{SS}}$	$\nu_{\sigma_{SS}}$
2.0–3.0	1.287	1.940	1.629	0.957	1.189
3.0–4.0	1.172	1.651	1.071	1.074	1.195
4.0–5.0	1.075	1.194	0.983	1.076	1.097
5.0–6.0	0.950	0.812	1.204	0.889	0.876
6.0–7.3	0.958	0.963	1.363	0.798	0.829

These factors should be multiplied with the sigma values taken from Table 5 if magnitude-specific uncertainty is required.

only a minor effect on the average V/H ratio estimates. Such a conclusion might appear to be controversial, and it is still under debate. In reality, a certain dependence on magnitude might be present on V/H spectral ratios, and in theory it should not be neglected. As a matter of fact, increasing magnitudes would affect a progressively deeper portion of the crust, influencing the way the wave field interacts with the surface (and thus the development of the surface waves). However, this effect is generally stronger in the very near field, where on the other side we lack of sufficient data. In the intermediate to far field, such effect might also be present, but from the analysis of our dataset it appears to be negligible when compared to the leading influence of the local site conditions and the distance dependence.

In this study, using the Japanese KiK-net database, we calibrated the regression coefficients in the range between 0.5 and 100 Hz. Because of practical limitations of the profile resolution and the recording's SNR, however, the range 1–10 Hz was considered as the most reliable for the correlation of quarter-wavelength properties and V/H. Higher and lower frequencies were nevertheless extrapolated from the available range without any loss of generality using an

empirical calibration approach. Back-computations of V/H response spectral ratios at target sites of the Japanese network showed that the main features of the curves can be reproduced, including resonance troughs and peaks. An adequate level of knowledge of the velocity profile at the site is nevertheless a prerequisite. For progressively stiffer sites ($V_{S30} > 700$ m/s), where resonance effects become less critical, results of this analysis were shown to be consistent with what was found in Edwards *et al.* (2011). Finally, the regression coefficients have been successfully used to model the V/H ratios at four strong-motion station sites in Switzerland (SBAF, SMZW, ZUR, and VISP2). The results are consistent with the observed response spectral ratios in the range 0.5 Hz to PGA, with the only exception of VISP2; in this case, we suspect a major role of 2D basin effects and edge-generated surface waves, which cannot be modeled by the proposed method.

As main limitation of such a procedure, a mismatch between resonance frequencies estimated from the IC curve (and thus from velocity profile) and from direct observation might exist, which directly affects the computation of the V/H spectral ratios. As a working hypothesis, we assume that such a mismatch—as observed in some sites of the Japanese network—is principally induced by an inadequate representation of the measured velocity profile (e.g., by biased positioning of the main seismic interfaces and an insufficient resolution depth). As a consequence, a reliable and sufficiently accurate assessment of the S-wave velocity structure down to an adequate depth is required. This is directly related to the lowest investigated frequency. This information is however not always available in practice, due to the high costs of most common investigation approaches. In this context, however, the combined use of active surface techniques and passive ambient vibration techniques can be advantageous, as it gives the possibility to obtain sufficiently accurate estimates of the velocity profiles at very shallow (from active) and rather great depths (from passive, in the order of hundreds of meters) with a relatively limited investment.

An advantage of the use of V/H ratios in PSHA is the fact that this approach enforces disaggregation-scenario compatible spectra for both the horizontal and vertical components. Gülerce and Abrahamson (2011) presented a detailed discussion of the merits and limitations of different approaches for constructing the vertical design spectrum through the combination of the uniform hazard or conditional mean spectrum (UHS or CMS, respectively) with the V/H ratio. They concluded that, given a structural response more sensitive to horizontal than vertical motions, the best approach is to develop a vertical CMS, conditioned on the horizontal CMS at the reference spectral period T_0 . The covariance matrix between horizontal and vertical ground-motion residuals is then used to account for the correlation of variability in the horizontal and vertical ground motions. In this way, the vertical CMS is consistent with the horizontal CMS, while accounting for the correlation of horizontal and vertical ground motions. In

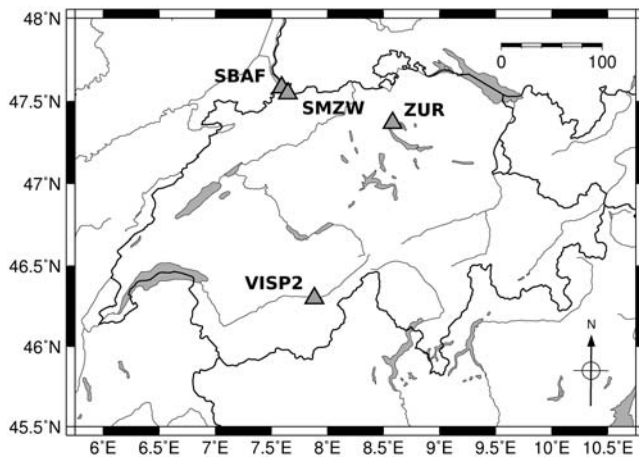


Figure 16. Location of the four investigated sites (SBAF, SMZW, ZUR, and VISP2) in Switzerland. For each station, a velocity profile is available from the site characterization database of SED.

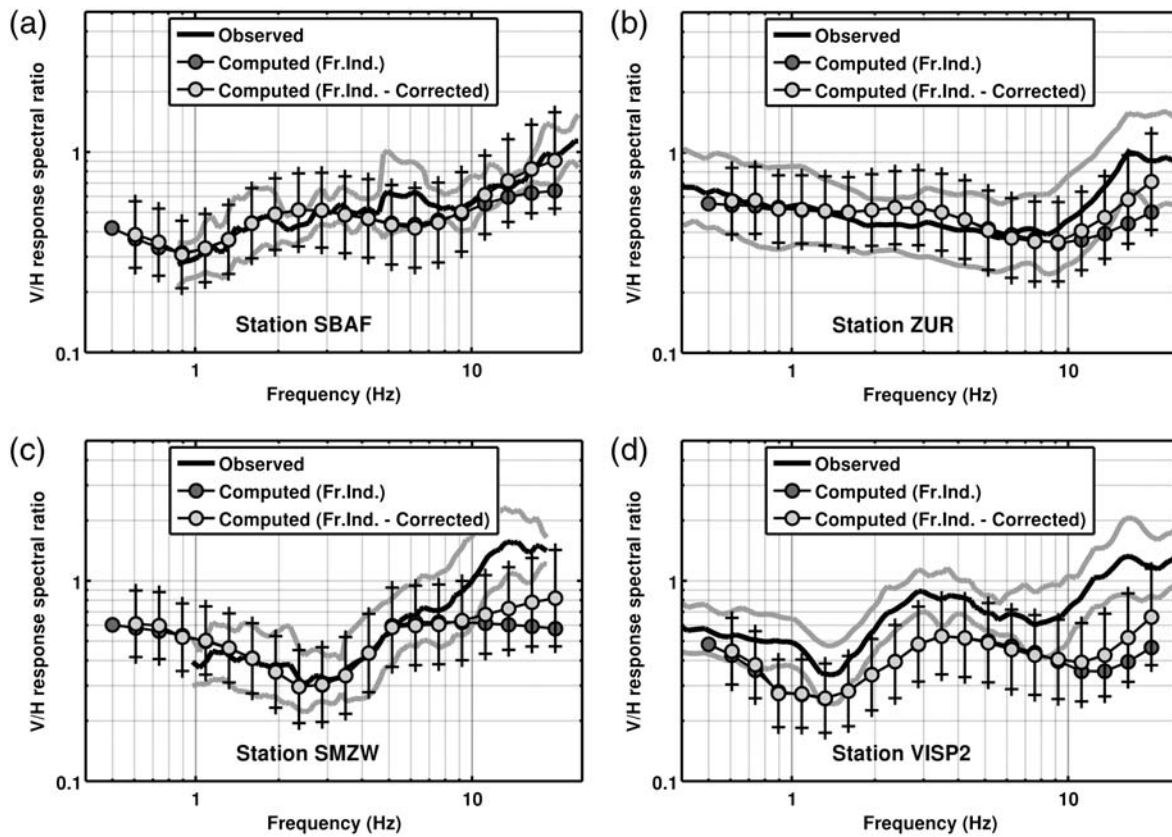


Figure 17. Comparison between back-computed V/H (dark gray dotted line) and observations (black solid line) using the frequency-independent correlations at the four Swiss test sites. The result of applying the frequency-dependent correction (light gray dotted line) is also presented. (a) $V_{S30} = 378$ m/s, (b) $V_{S30} = 635$ m/s, (c) $V_{S30} = 483$ m/s, (d) $V_{S30} = 232$ m/s.

order to produce the CMS using the V/H ratio presented in this study, we suggest implementing the covariance matrices presented by Gülerce and Abrahamson (2011). On the other hand, given a structural response more sensitive to vertical motions, Gülerce and Abrahamson (2011) recommend that it is more appropriate to directly scale the UHS with the V/H ratio, as it better represents the vertical hazard. A site-specific V/H as developed in our work is highly beneficial and properly represents the resonance features of the site.

Data and Resources

The Japanese earthquake data and velocity profiles are available through the NIED ftp service (www.kik.bosai.go.jp/, last accessed January 2011). Velocity profiles of the Swiss stations SBAF, SMZW, ZUR, and VSIP2 are part of the site characterization database of the Swiss Seismological Service (SED) (available upon request). The Swiss earthquake recordings used for defining site V/H ratios have been extracted from the recording database of SED through AutoDRM

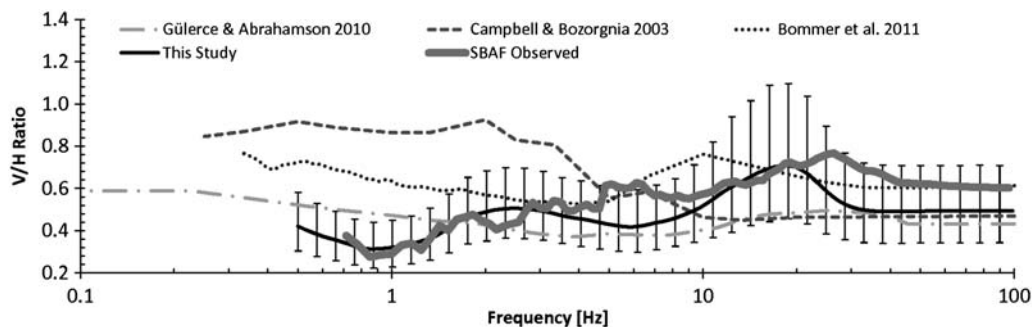


Figure 18. Comparison between V/H predicted using different approaches available in the literature (Campbell and Bozorgnia, 2003; Bommer *et al.*, 2011; Gülerce and Abrahamson, 2011) at Swiss strong-motion installation site SBAF ($V_{S30} = 379$ m/s) for M 5 at 80 km, including sigma.

(www.seismo.ethz.ch/prod/autodrm/index_EN, last accessed January 2011) or via the ArcLink web-interface (<http://arclink.ethz.ch/>, last accessed January 2011). Figure 16 in this paper was made using Generic Mapping Tools (GMT) 4 software written by Wessel and Smith (1998).

Acknowledgments

We thank the NIED for making waveform and velocity profile data available. This work was partly funded by *Swissnuclear* through the PRP Project (Renault *et al.*, 2010) and the Swiss Federal Nuclear Safety Inspectorate (ENSI). We would also like to thank Associate Editor Martin Chapman and two anonymous reviewers.

References

- Akkar, S., and J. J. Bommer (2006). Influence of long-period filter cut-off on elastic spectral displacements, *Earthquake Eng. Struct. Dynam.* **35**, no. 9, 1145–1165.
- Al Atik, L., N. Abrahamson, J. J. Bommer, F. Scherbaum, F. Cotton, and N. Kuehn (2010). The variability of ground-motion and its components, *Seismol. Res. Lett.* **81**, no. 5, 794–801.
- Aoi, S., T. Kunugi, and H. Fujiwara (2004). Strong-motion seismograph network operated by NIED: K-NET and KiK-net, *J. Jpn. Assoc. Earthquake Eng.* **4**, 65–74.
- Atkinson, G. M. (2006). Single-station sigma, *Bull. Seismol. Soc. Am.* **96**, 446–455.
- Baker, J. W., and C. A. Cornell (2006). Spectral shape, epsilon and record selection, *Earthquake Eng. Struct. Dynam.* **35**, no. 9, 1077–1095.
- Bard, P.-Y., and M. Bouchon (1985). The two-dimensional resonance of sediment-filled valleys, *Bull. seismol. Soc. Am.* **75**, no. 2, 519–541.
- Bommer, J. J., S. Akkar, and Ö. Kale (2011). A Model for vertical-to-horizontal response spectral ratios for Europe and the Middle East, *Bull. Seismol. Soc. Am.* **101**, no. 4, 1783–1806.
- Boore, D. (2003). Simulation of ground motion using the stochastic method, *Pure Appl. Geophys.* **160**, no. 3–4, 635–676.
- Campbell, K. W. (1997). Empirical near-source attenuation relationships for horizontal and vertical components of peak ground acceleration, peak ground velocity, and pseudo-absolute acceleration response spectra, *Seismol. Res. Lett.* **68**, no. 1, 154–179.
- Campbell, K. W., and Y. Bozorgnia (2003). Updated near-source ground-motion (attenuation) relations for the horizontal and vertical components of peak ground acceleration and acceleration response spectra, *Seismol. Soc. Am.* **93**, 1872–1872.
- Deichmann, N., J. Clinton, S. Husen, B. Edwards, F. Haslinger, D. Fäh, D. Giardini, P. Kästli, U. Kradolfer, I. Marschall, and S. Wiemer (2010). Earthquakes in Switzerland and surrounding regions during 2009, *Swiss J. Geosci.* **103**, no. 3, 535–549.
- Delavaud, E., F. Cotton, S. Akkar, F. Scherbaum, L. Danciu, C. Beauval, S. Drouet, J. Douglas, R. Basili, M. A. Sandikkaya, M. Segou, E. Faccioli, and N. Theodoulidis (2012). Toward a ground-motion logic tree for probabilistic seismic hazard assessment in Europe, *J. Seismol.* **16**, no. 3, 451–473.
- Douglas, J., and D. M. Boore (2010). High-frequency filtering of strong motion records, *Bull. Earthquake Eng.* **9**, 395–409.
- Edwards, B., B. Allmann, D. Fäh, and J. Clinton (2010). Automatic computation of moment magnitudes for small earthquakes and the scaling of local to moment magnitude, *Geophys. J. Int.* **183**, no. 1, 407–420.
- Edwards, B., V. Poggi, and D. Fäh (2011). A Predictive Equation for the vertical-to-horizontal ratio of ground motion at rock sites based on shear-wave velocity profiles from Japan and Switzerland, *Bull. Seismol. Soc. Am.* **101**, no. 6, 2998–3019.
- Edwards, B., A. Rietbrock, J. J. Bommer, and B. Baptie (2008). The acquisition of source, path, and site effects from microearthquake recordings using Q tomography: Application to the United Kingdom, *Bull. Seismol. Soc. Am.* **98**, no. 4, 1915–1935.
- Fäh, D., S. Fritsche, V. Poggi, G. Gassner-Stamm, P. Kästli, J. Burjanek, P. Zweifel, S. Barman, J. Clinton, L. Keller, P. Renault, and S. Heuberger (2009). Determination of site information for seismic stations in Switzerland, Swiss Seismological Service Technical Report: SED/PRP/R/004/20090831, for the *swissnuclear* Pegasos Refinement Project.
- Fäh, D., J. Moore, J. Burjanek, I. Iosifescu, L. Dalguer, F. Dupray, C. Michel, J. Woessner, A. Villiger, J. Laue, I. Marschall, V. Gischig, S. Loew, S. Alvarez, W. Balderer, P. Kästli, G. Giardini, C. Iosifescu, L. Humi, P. Lestuzzi, A. Karbassi, C. Baumann, A. Geiger, A. Ferrari, L. Laloui, J. Clinton, and N. Deichmann (2012). Coupled seismogenic geohazards in alpine regions, *Bolletino di Geofisica Teorica ed Applicata*, in press.
- Fäh, D., G. Stamm, and H.-B. Havenith (2008). Analysis of three-component ambient vibration array measurements, *Geophys. J. Int.* **172**, no. 1, 199–213.
- Gülerce, Z., and N. A. Abrahamson (2010). Vector-valued probabilistic seismic hazard assessment for the effects of vertical ground motions on the seismic response of highway bridges, *Earthquake Spectra* **26**, 999–1016.
- Gülerce, Z., and N. A. Abrahamson (2011). Site-specific design spectra for vertical ground-motion, *Earthquake Spectra* **27**, no. 4, 1023–1047.
- Havenith, H.-B., D. Fäh, U. Polom, and A. Roulle (2007). S-wave velocity measurements applied to the seismic microzonation of Basel, Upper Rhine Graben, *Geophys. J. Int.* **170**, no. 1, 346–358.
- Joyner, W. B., R. E. Warrick, and T. E. Fumal (1981). The effect of Quaternary alluvium on strong ground motion in the Coyote Lake, California, earthquake of 1979, *Bull. Seismol. Soc. Am.* **71**, no. 4, 1333–1349.
- Kunnath, S. K., E. Erduran, Y. H. Chai, and M. Yashinsky (2008). Effect of near-fault vertical ground motions on seismic response of high overcrossings, *J. Bridge Eng.* **13**, no. 3, 282–290.
- Lagarias, J. C., J. A. Reeds, M. H. Wright, and P. E. Wright (1998). Convergence properties of the Nelder—Mead simplex method in low dimensions, *SIAM J. Optim.* **9**, no. 1, 112–147.
- Poggi, V., and D. Fäh (2010). Estimating Rayleigh wave particle motion from three-component array analysis of ambient vibrations, *Geophys. J. Int.* **180**, no. 1, 251–267.
- Poggi, V., B. Edwards, and D. Fäh, (2011). Derivation of a reference shear-wave velocity model from empirical site amplification, *Bull. Seismol. Soc. Am.* **101**, no. 1, 258–274.
- Renault, P., S. Heuberger, and N. A. Abrahamson (2010). PEGASOS Refinement Project: An improved PSHA for Swiss nuclear power plants, in *Proceedings of 14ECEE—European Conference of Earthquake Engineering*, Ohrid, Republic of Macedonia, Paper ID. 991.
- Roten, D., D. Fäh, K. B. Olsen, and D. Giardini (2008). A comparison of observed and simulated site response in the Rhône valley, *Geophys. J. Int.* **173**, no. 3, 958–978.
- Scherbaum, F., K.-G. Hinzen, and M. Ohrnberger (2003). Determination of shallow shear wave velocity profiles in the Cologne Germany area using ambient vibrations, *Geophys. J. Int.* **152**, no. 3, 597–612.
- Wessel, P., and W. H. F. Smith (1998). New, improved version of the Generic Mapping Tools released, EOS, *Trans. Am. Geophys. Union*, **79**, 579.

Swiss Seismological Service
Sonneggstrasse, 5
ETH Zürich
Zürich, Switzerland
poggi@sed.ethz.ch